MOLECULAR AND CELLULAR BIOLOGY, Aug. 2008, p. 4745–4758 Vol. 28, No. 15
0270-7306/08/$08.00+0 doi:10.1128/MCB.01747-07

Regulation of p53 Target Gene Expression by Peptidylarginine Deiminase 4▽†

Pingxin Li,[1] Hongjie Yao,[1] Zhiqiang Zhang,[1] Ming Li,[1] Yuan Luo,[2] Paul R. Thompson,[2] David S. Gilmour,[1] and Yanming Wang[1]*

Center for Gene Regulation, Department of Biochemistry and Molecular Biology, Pennsylvania State University, University Park, Pennsylvania 16802,[1] and Department of Chemistry and Biochemistry, University of South Carolina, 631 Sumter Street, Columbia, South Carolina 29208[2]

Received 24 September 2007/Returned for modification 27 November 2007/Accepted 20 May 2008

Histone Arg methylation has been correlated with transcriptional activation of p53 target genes. However, whether this modification is reversed to repress the expression of p53 target genes is unclear. Here, we report that peptidylarginine deiminase 4, a histone citrullination enzyme, is involved in the repression of p53 target genes. Inhibition or depletion of PAD4 elevated the expression of a subset of p53 target genes, including p21/CIP1/WAF1, leading to cell cycle arrest and apoptosis. Moreover, the induction of p21, cell cycle arrest, and apoptosis by PAD4 depletion is p53 dependent. Protein-protein interaction studies showed an interaction between p53 and PAD4. Chromatin immunoprecipitation assays showed that PAD4 is recruited to the p21 promoter in a p53-dependent manner. RNA polymerase II (Pol II) activities and the association of PAD4 are dynamically regulated at the p21 promoter during UV irradiation. Paused RNA Pol II and high levels of PAD4 were detected before UV treatment. At early time points after UV treatment, an increase of histone Arg methylation and a decrease of citrullination were correlated with a transient activation of p21. At later times after UV irradiation, a loss of RNA Pol II and an increase of PAD4 were detected at the p21 promoter. The dynamics of RNA Pol II activities after UV treatment were further corroborated by permanganate footprinting. Together, these results suggest a role of PAD4 in the regulation of p53 target gene expression.

In eukaryotic cells, 147 bp of DNA is wrapped around a core histone octamer (including two each of histones H3, H2B, H2A, and H4) to form a nucleosome core particle, the basic structural unit of chromatin (52). Posttranslational histone modifications, including methylation, acetylation, phosphorylation, ubiquitination, and citrullination, have been found to play a major role in chromatin functions, such as transcription (5, 7, 35, 39, 55). Moreover, specialized protein domains, including chromo-, bromo-, and tudor domains and PHD fingers, have evolved to recognize histone modification "marks" and to regulate nuclear events following histone modifications (33, 36, 40). Histone Arg methylation is catalyzed by members of the protein Arg methyltransferase (PRMT) family (11, 57, 61). The methylation of histones H3 and H4 has been correlated with the expression of nuclear receptor target genes and developmentally regulated genes (6, 30). In searching for enzymes that can reverse histone Arg methylation, we and others previously reported that a histone Arg demethylimination enzyme, PAD4 (also called PADI4), can convert both Arg and monomethyl-Arg to citrulline, thereby regulating histone Arg methylation (14, 35, 62). In contrast to the role of histone Arg methylation in transcriptional activation, the demethylimination and citrullination of histones mediated by PAD4 have been found to play a role in transcriptional repression of nuclear receptor target genes (3, 14, 62). Several mechanisms can be envisioned to explain the functions of histone demethylimination and citrullination. First, demethylimination by PAD4 directly decreases the amount of methyl-Arg on histones; second, citrulline residues cannot serve as the PRMT substrate, thereby preventing the PRMT function; third, citrulline can be recognized by effector proteins that regulate chromatin functions.

The tumor suppressor p53 plays a pivotal role in regulating the cell cycle progression and apoptosis in response to various genotoxic and nongenotoxic stresses (37, 51, 59). The ability of p53 to function as a sequence-specific transcription factor is critical for its tumor suppressor function. Hundreds of p53 target genes have been identified (25, 37, 59). These include genes inducing cell cycle arrest, such as p21/WAF1/CIP1 and GADD45, an E3 ubiquitin ligase of p53-MDM2, as well as genes inducing apoptosis, such as PUMA, Bax, and PIG3 (59, 64). To facilitate the activation of its target genes, p53 recruits several histone acetyltransferases (e.g., p300/CBP, Tip60, and PCAF) (4, 8, 17, 45, 58). These acetyltransferases play multiple roles in the activation of p53 target genes by acetylating histones as well as p53 itself (4, 17, 20). In addition, p53 can repress transcription by recruiting corepressors, such as histone deacetylases 1 and 2 (HDAC1 and HDAC2), LSD1, and DNA methyltransferase (22, 27, 29, 37, 38). Consistent with a role of these proteins in the repression of p21, depletion of HDAC1, HDAC2, and LSD1 has been found to increase the expression of p21 in cells without exposure to DNA damage (23, 29, 54).

Recently, protein Arg methyltransferases PRMT1 and CARM1 were found to regulate the expression of p53 target

* Corresponding author. Mailing address: Center for Gene Regulation, Department of Biochemistry and Molecular Biology, Pennsylvania State University, University Park, PA 16802. Phone: (814) 865-3775. Fax: (814) 865-7770. E-mail: yuw12@psu.edu.

† Supplemental material for this article may be found at http://mcb.asm.org/.

▽ Published ahead of print on 27 May 2008.

genes (1). An increase of histone Arg methylation was followed by a decrease of this modification on the GADD45 promoter after UV irradiation (1). How histone Arg methylation is reversed during p53 target gene expression is unknown. Because PAD4 can convert both monomethyl-Arg and Arg in histones to citrulline, we investigated whether PAD4 plays a role in the p53 pathway to regulate gene expression. Here, we report that inhibition or depletion of PAD4 induces the expression of p21 in a p53-dependent manner. PAD4 interacts with p53 and is recruited to the p21 promoter to regulate histone Arg methylation and citrullination. Our studies suggest that p53 plays multifaceted roles in gene regulation by interacting with transcriptional coactivators or corepressors to fine-tune the expression of its target genes.

MATERIALS AND METHODS

Molecular biology and plasmid constructs. Flag-p53 was cloned into the pIRES vector for expression in human cell lines. Glutathione *S*-transferase (GST)–PAD4, GST-PAD4$^{IL\text{-}1\&2}$, GST-PAD4$^{IL\text{-}1}$, GST-p53, GST-p53$^{1–300}$, and GST-p53$^{301–393}$ were cloned in the pGEX4T1 vector for expression in *Escherichia coli* strain BL21. Flag-His6-p53 was cloned into pET11a vector for expression in *E. coli*. The pSG5-PAD4 construct and the pSG5-PAD4C645S mutant construct were described previously (62). To establish Flag-hemagglutinin (HA)-PAD4-expressing 293T and MCF-7 cell lines, Flag-HA-PAD4 was cloned into the pMIGR1 vector (49). All constructs were confirmed by DNA sequencing at the Nucleic Acid Facility of Penn State University. Primers for cloning and constructs are available upon request.

Cell culture and treatments with siRNAs, shRNA, Cl-amidine, doxorubicin, and UVC. 293T, p53$^{-/-}$ H1299, MCF-7, and U2OS cells were cultured in Dulbecco modified Eagle medium supplemented with 10% fetal bovine serum and 1% penicillin-streptomycin in a 5% CO_2 incubator. HCT116 p53$^{+/+}$ and p53$^{-/-}$ cells were cultured in McCoy's 5A medium supplemented with 10% fetal bovine serum and 1% penicillin-streptomycin in a 5% CO_2 incubator. PAD4 SMARTpool small interfering RNAs (siRNAs) were purchased from Dharmacon Inc. A green fluorescent protein (GFP) siRNA (Dharmacon Inc.) was used as a control for the siRNA experiments. siRNAs were transfected using the XtremeGene siRNA transfection reagents (Roche Inc.). Cells were incubated in the presence of the siRNAs for 60 h before analyses. To make the PAD4 short hairpin RNA (shRNA) construct, annealed short hairpin oligonucleotides targeting nucleotides 547 to 565 (5′-GCGAAGACCTGCAGGACAT-3′) of PAD4 mRNA sequence (NCBI accession no. NM_012387) were cloned into the pHTP vector (60). For the p53 shRNA construct, annealed short hairpin oligonucleotides targeting nucleotides 1026 to 1044 (5′-GACTCCAGTGGTAATCTAC-3′) of the p53 mRNA sequence (NCBI accession no. NM_000546.3) were cloned into the pHTP vector. At 12 h after transfection of the shRNA plasmid with Lipofectamine 2000, fresh medium containing 3 μg/ml puromycin was added to select transfected cells for 6 days before reverse transcription-PCR (RT-PCR), Western blotting, and flow cytometry analyses. Due to the cell growth disadvantage after PAD4 depletion, each repeat experiment with the PAD4 shRNA was performed using freshly transformed cells. To analyze the effects of doxorubicin on p21 expression, 0.5 μM of doxorubicin (Sigma-Aldrich) was added to treat cells for 6 h. Cl-amidine was dissolved in H_2O as a 10 mM stock solution and diluted to 200 μM in the complete cell culture medium to treat cells in six-well plates. Cells were collected at different time points as indicated in the text after Cl-amidine treatment before RT-PCR and Western blot analyses. For UV irradiation, cells were exposed to 50 J/m^2 of UVC light in a Spectrolinker XL-1000 UV cross-linker (Spectronics Inc.). To analyze cell number changes, 10,000 cells/well were plated in the six-well plates. The Cl-amidine, PAD4 siRNA, or GFP siRNA treatment was performed in triplicate. At 72 h after Cl-amidine treatment or 60 h after PAD4 siRNA treatment, cells were trypsinized and counted using a hepatocytometer. The numbers of cells in the wells without Cl-amidine treatment or with GFP siRNA treatment were normalized to 100%, and the percentage of cell number decrease was calculated by dividing the number of cells after Cl-amidine treatment or PAD4 siRNA treatment by that of the respective control groups and then multiplying that value by 100. Standard deviations were calculated using the Microsoft Excel program.

Western blotting and RT-PCR. To detect histone citrullination by GST-PAD4, Cl-amidine at various concentrations was incubated with 0.5 μg of GST-PAD4 for 10 min in the PAD assay buffer (Tris-HCl, pH 7.6, 4 mM dithiothreitol, 4 mM $CaCl_2$, 1 mM phenylmethylsulfonyl fluoride) before 2 μg of purified histone H3 was added and further incubated for 1 h at 37°C. Western blotting using the anti-Mod-Cit antibody (17-347; Upstate Biotechnology Inc.) was performed essentially as previously described (62). Other antibodies used for Western blotting included anti-PAD4, a rabbit polyclonal antibody made against a GST-PAD4 fusion protein, anti-p53 monoclonal antibody (clone BP53-12; Sigma), anti-p53 phospho-Ser15 (catalog no. 92 86; Cell Signaling), anti-p21 (P1484; Sigma), anti-H3R17Me (Ab8284; Abcam), H3Cit (Ab5103; Abcam), anti-HA (H9658; Sigma), anti-β-tubulin (T8535; Sigma), anti-histone H3 (Ab1791; Abcam), and antiactin (A4700; Sigma) at appropriate dilutions. After incubation with the appropriate horseradish peroxidase-conjugated secondary antibody, signals were detected using the Lumi-Light^{PLUS} Western blotting substrate (Roche).

For RT-PCR, total RNA was extracted from cells by using the RNeasy minikit (catalog no. 74104; Qiagen). RNA concentrations were measured and normalized using the amount of 18S rRNA. Equal amounts of RNA (0.2 μg) were used to perform RT-PCR using the Superscript One-Step RT-PCR kit (10928-042; Invitrogen). Primers used for RT-PCR included p21-RT-forward (5′-TCTTGTACC CTTGTGCCTC-3′), p21-RT-reverse (5′-AACCTCTCATTCAACCGCC-3′), GADD45-RT-forward (5′-AACGACATCAACATCCTGC-3′), GADD45-RT-reverse (5′-CCTTCTTCATTTTCACCTCTTTCC-3′), CDC25C-RT-forward (5′-TGGGGAGATAACTGCCACTC-3′), CDC25C-RT-reverse (5′-GC TTCAGTCTTGGCCTGTTC-3′), MDM2-RT-forward (5′-TGGTTGGATC AGGATTCAGT-3′), MDM2-RT-reverse (5′-TTCCAGTTTGGCTTTCTCAG-3′), PUMA-RT-forward (5′-TGTGAATCCTGTGCTCTGCC-3′), PURMA-RT-reverse (5′-TTCCGGTATCTACAGCAGCG-3′), GAPDH-RT-forward (5′-CGA GATCCCTCCAAAATCAA-3′), and GAPDH-RT-reverse (5′-TGTGGTCATGA GTCCTTCCA-3′). PCR signals were detected between 26 and 32 cycles on agarose gels. Gel images were analyzed using the NIH Image J program to quantify the amount of signals.

Immunostaining, TUNEL, and flow cytometry assays. Cell staining was carried out essentially as previously described (62). For double labeling with terminal deoxynucleotidyltransferase-mediated dUTP-biotin nick end labeling (TUNEL) and antibody, cells were first fixed with 3.7% paraformaldehyde and TUNEL staining was performed with a DeadEnd Fluorometric TUNEL kit (catalog no. G3250; Promega Inc.) per the manufacturer's instructions. Following TUNEL staining, cells were washed with PBST (phosphate-buffered saline [PBS] with 0.1% Triton X-100), blocked with 2% bovine serum albumin, and stained with the PAD4 antibody (1:200) and a goat anti-rabbit Cy3-labeled secondary antibody (1:1,000). Nuclei were visualized by DNA staining with Hoechst stain (1 μg/ml). The images were captured using a Zeiss Axioskop 40 fluorescence microscope. The number of nuclei stained by Hoechst stain, TUNEL, or PAD4 was counted from randomly selected fields. To analyze the percentage of apoptotic cells in the p53$^{+/+}$ and p53$^{-/-}$ HCT116 cells transfected with the PAD4 shRNA or the pHTP vector, cells were stained with annexin V (556418; BD Biosciences) and analyzed by flow cytometry. Briefly, the cells from different treatment groups were trypsinized and washed twice with the annexin V binding buffer (10 mM HEPES, pH 7.4, 2.5 mM $CaCl_2$, 140 mM NaCl, 5 mM KCl, 1 mM $MgCl_2$). Cells (5×10^5) were resuspended in 200 μl of binding buffer and stained with fluorescein isothiocyanate-conjugated annexin V in the dark for 20 min at room temperature. At least 1×10^4 cells were counted to analyze the intensity of annexin V staining using the FC500 flow cytometer (Beckman Coulter) and the CXP software at the Penn State Flow Cytometry Facility. To analyze the cell cycle profiles, trypsinized cells were first fixed with cold 70% ethanol for 5 min. Cells were pelleted and then resuspended and rehydrated in PBS for 15 min. After treatment with RNase A for 30 min and staining with 20 μg/ml propidium iodide for 30 min at room temperature, at least 1×10^4 cells were analyzed by the FC500 flow cytometer. Cells were gated to exclude cell debris and/or sub-G_1 cells during cell cycle analyses.

Establishment of FH-PAD4-expressing 293T and MCF-7 cell lines. The PAD4 cDNA with N-terminal Flag and HA tags (FH-PAD4) was cloned into the retrovirus pMIGR1 vector. Stable FH-PAD4-expressing 293T and MCF-7 cell lines were established by retrovirus spinoculation as previously described (49). Briefly, FH-PAD4/pMIGR1 and ψ_{amplo} plasmids were cotransfected into 293T cells to produce retrovirus. The retrovirus in the supernatant was filtered with an 0.45-μm-pore-size filter and was used to infect 293T or MCF-7 cells. FH-PAD4 and GFP were produced from the same bicistronic transcript. GFP-positive cells were enriched by fluorescence-activated cell sorting twice so that over 90% of cells were GFP and FH-PAD4 positive. The percentage of GFP-positive cells was routinely checked using a Zeiss fluorescence microscope.

Nuclear extract preparations, coimmunoprecipitation, and GST pull-down. Nuclear extracts were prepared following a protocol from R. Roeder's laboratory (Rockefeller University) with slight modifications. Briefly, about 1×10^8 293T cells or 293T cells expressing FH-PAD4 were collected by scraping to detach the

cells from the dishes. Cells were washed twice with PBS and once with hypotonic solution (10 mM Tris-HCl, pH 7.3, 10 mM KCl, 1.5 mM $MgCl_2$ supplemented with protease inhibitors). The cells were then swelled in 5 ml of hypotonic solution for 10 min and homogenized in a Dounce homogenizer for 15 strokes with a tight pestle. Cell lysis was checked under a microscope. Nuclei were collected by centrifugation at 3,000 rpm for 10 min at 4°C and then extracted with high-salt buffer (20 mM Tris-HCl, pH 7.3, 600 mM KCl, 1.5 mM $MgCl_2$, 0.2 mM EDTA, 25% glycerol, with protease inhibitors). The extracted nuclear proteins were dialyzed against a medium-salt buffer (20 mM Tris-HCl, pH 7.3, 300 mM KCl, 1.5 mM $MgCl_2$, 0.2 mM EDTA, 25% glycerol, with 1 mM phenylmethylsulfonyl fluoride). For coimmunoprecipitation of p53 with Flag-PAD4, M2 agarose beads (Sigma; A2220) were incubated with the nuclear extracts at 4°C overnight, washed three times with the medium-salt buffer, and finally washed with Tris-buffered saline. For coimmunoprecipitation of PAD4 with the p53 antibody, the 293T nuclear extracts were loaded on an 11-ml 5 to 30% sucrose gradient in PBS buffer supplemented with protease inhibitors and centrifuged using a Beckman SW28 rotor at 26,000 rpm for 16 h. Fractions were collected from the top of the sucrose gradient. Fractions containing both p53 and PAD4 were pooled and used for coimmunoprecipitation following a previously published protocol (31). For coimmunoprecipitation of p53 by the PAD4 antibody, 293 nuclear extracts were used. GST pull-down was performed essentially as previously described (31).

Permanganate footprinting and LM-PCR. U2OS cells (2×10^6) were washed with PBS and suspended in 100 μl PBS. Cells were treated with permanganate by adding 100 μl of 20 mM $KMnO_4$ dissolved in PBS. The permanganate reaction mixture was incubated on ice for 1 min and stopped by the addition of 200 μl of stop solution (20 mM Tris-HCl, pH 7.5, 20 mM NaCl, 40 mM EDTA, 1% sodium dodecyl sulfate, 400 mM 2-mercaptoethanol). The solution was vigorously shaken until all coloration had vanished. Each sample was treated with 50 μg of proteinase K for at least 1 h and then sequentially extracted with phenol, phenol-chloroform-isoamyl alcohol (49.5:49.5:1), and chloroform. DNA was precipitated with 0.3 M sodium acetate (pH 6.0) and ethanol. The DNA pellets were washed with 75% ethanol and dissolved in 20 μl Tris-EDTA (TE; pH 7.5). To determine the pattern of permanganate reactivity, 500 ng of each DNA sample was diluted in 15 μl TE (pH 7.5). H_2O (75 μl) and piperidine (10 μl) were then added, and each sample was incubated at 90°C for 30 min. Three hundred microliters of H_2O was added to each sample, and then the samples were extracted three times with 700 μl isobutanol and once with ether. The volume of the DNA was adjusted to 100 μl with H_2O, and then the DNA was precipitated with ethanol. The DNA was dissolved in 10 μl TE (pH 7.5), transferred to a fresh siliconized tube, and further analyzed by ligation-mediated PCR (LM-PCR) (9). LM-PCR was performed with a set of nested primers, LM-1, LM-2, and LM-3. These primers span the region +235 to +188 nucleotides downstream from the transcription start site of the p21 gene. The sequence and annealing temperature used in the PCR for each of these primers were as follows: LM-1, 5′-TTCACCTGCCGCAGAAAC-3′ (61°C); LM-2, 5′-AGAAACACCTGTGAACGCAGCA-3′ (65°C); and LM-3, 5′-CAGCACACACCCGCGAACA-3′ (68°C).

ChIP. Chromatin immunoprecipitation (ChIP) experiments were carried out essentially as previously described with minor alterations (62). The chromatin was fragmented to a range of 0.5 to 1 kb after sonication with a Bioruptor (Diagenode Inc.). After the ChIP procedures, the ChIP DNA samples were purified using the Qiagen PCR product purification kit. The PCR primers used to amplify the p21 promoter spanned p53 binding site 2 of the promoter, including p21-ChIP-forward (5′-CCAGCCCTTGGATGGTTT-3′) and p21-ChIP-reverse (5′-GCCTCCTTTCTGTGCCTGA-3′). The PCR primers used to amplify the glyceraldehyde-3-phosphate dehydrogenase (GAPDH) promoter were GAPDH-ChIP-forward (5′-CAATTCCCCATCTCAGTCGT-3′) and GAPDH-ChIP-reverse (5′-TAGTAGCCGGGCCCTACTTT-3′). PCR products were analyzed between cycles 29 and 34 of the PCRs. The PCR results shown were representative of three independent ChIP experiments. Real-time quantitative PCRs (Q-PCRs) were performed using the Sybr green reagent (4367659; Applied Biosystems). The Q-PCR primers to detect p53 binding site 1 were forward (5′-AGCAGGCTGTGGCTCTGATT-3′) and reverse (5′-CAAAATAGCCACCAGCCTCTTCT-3′). The Q-PCR primers to detect p53 binding site 2 were forward (5′-CTGTCCTCCCCGAGGTCA-3′) and reverse (5′-ACARCRCAGGCTGCTCAGAGTCT-3′). The Q-PCR primers to detect the +182 region of p21 were forward (5′-CGTGTTCGCGGGTGTGT-3′) and reverse (5′-CATTCACCTGCCGCAGAAA-3′). These primers have been used to perform Q-PCR in a previous study (19). Antibodies used for ChIP include anti-RNA polymerase II (Pol II; 8WG16; Covance; MMS-126R), anti-RNA Pol II Ser5 phosphorylation (H14; Covance; MMS-134R), anti-H3R17Me (Ab8284; Abcam), anti-H3Cit (Ab5103; Abcam), and anti-histone H3 (Ab1791; Abcam).

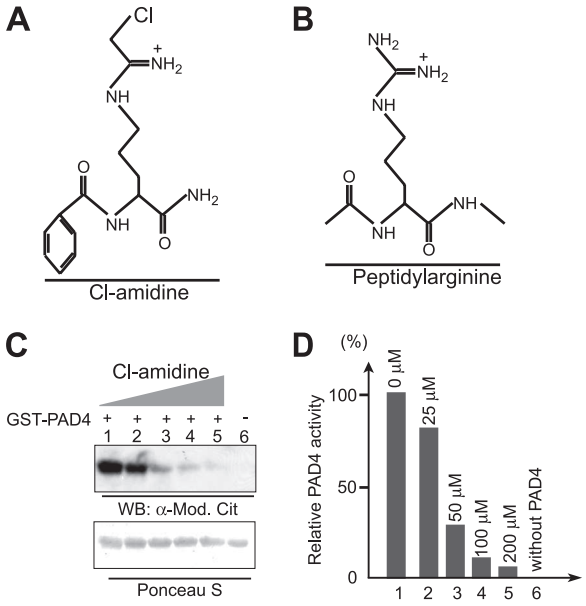

FIG. 1. PAD4 inhibitor Cl-amidine inhibits the activity of PAD4. (A and B) The structure of Cl-amidine (A) is similar to that of the PAD4 substrate peptidylarginine (B). (C) The activity of GST-PAD4 in histone citrullination was inhibited by preincubating GST-PAD4 with Cl-amidine. (D) The amount of histone citrullination signal detected in panel C was quantified using the NIH Image J program and graphed, with the concentration of the inhibitor indicated.

RESULTS

PAD4 inhibitor Cl-amidine activates the expression of the p53 target gene p21. Recently, a PAD4 inhibitor, Cl-amidine (Fig. 1A), was generated (42). Cl-amidine is structurally similar to the PAD4 substrate peptidylarginine (Fig. 1B) and inhibits PAD4 by covalent modification of a cysteine residue (Cys645) at the active site of the enzyme (42). As HDAC inhibitors have been widely used to study HDACs (22, 32), we postulated that Cl-amidine would be useful to study the cellular functions of PAD4. To test the effect of Cl-amidine in PAD4 inhibition, we first analyzed the ability of Cl-amidine to inhibit PAD4 activity by using histone H3 as a substrate in vitro and measured the efficacy of citrullination. Cl-amidine inhibited histone H3 citrullination by GST-PAD4 in a concentration-dependent manner (Fig. 1C and D). Under the experimental conditions applied, Cl-amidine inhibited more than 50% of the PAD4 activity at the 50 μM concentration, whereas over 90% inhibition was reached with 200 μM of Cl-amidine (Fig. 1D).

The dosage dependency of Cl-amidine inhibition of PAD4 in cells has been described using a reporter assay system (42). To test the effects of Cl-amidine and the inhibition of PAD4 on cell growth and proliferation, we treated the osteosarcoma U2OS cells with 200 μM of Cl-amidine. At 3 days after treatment, the number of Cl-amidine-treated cells was decreased to 48.3% ± 3.6% ($n = 3$) of that of the untreated cells (Fig. 2A). Western blotting found that the doublet bands of PAD4 in U2OS cells were unchanged after treatment with Cl-amidine (Fig. 2B), suggesting that Cl-amidine treatment did not affect the stability of PAD4. PAD4 was previously shown to convert methyl-Arg residues in histones to citrulline. If Cl-amidine

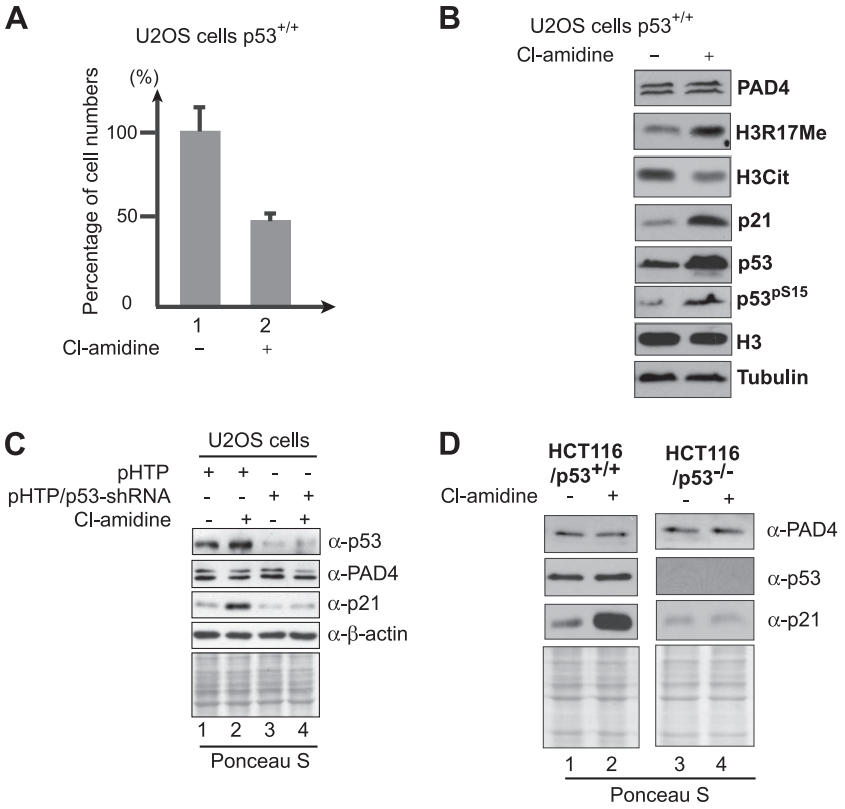

FIG. 2. Cl-amidine treatment increases p21 expression. (A) The number of U2OS cells treated with 200 μM of Cl-amidine was 48.3% ± 3.6% (n = 3) of the number of mock-treated cells, demonstrating that Cl-amidine has a negative effect on cell growth and proliferation. (B) Western blot analyses of the levels of PAD4, H3R17Me, H3Cit, p21, p53, and p53 Ser15 phosphorylation in U2OS cells after treatment with Cl-amidine for 24 h. The level of PAD4 was unaltered (note the doublet of PAD4 detected on the Western blot). Tubulin and histone H3 were monitored to ensure equal protein loading. (C) The effects of Cl-amidine on the expression of p21 in U2OS cells without or with the depletion of p53 using a pHTP/p53-shRNA plasmid. (D) Lanes 1 and 2, the changes of PAD4, p53, and p21 in the $p53^{+/+}$ HCT116 cells after the Cl-amidine treatment for 24 h detected by Western blotting. The p21 expression was increased by 7.7- ± 1.3-fold (n = 3). Lanes 3 and 4, changes in PAD4, p53, and p21 in the $p53^{-/-}$ HCT116 cells after the Cl-amidine treatment for 24 h. The increase in p21 expression was not observed.

inhibits PAD4 in cells, we postulated that histone citrullination would decrease, while histone Arg methylation would increase upon Cl-amidine treatment. In agreement, an ~2.2-fold increase of histone H3 Arg17 methylation as well as a ~50% decrease of histone H3 citrullination was detected (Fig. 2B).

Because histone Arg methylation has been correlated with the activation of p53-mediated transcription (1) and Cl-amidine treatment decreased cell growth (Fig. 2A), the expression of p21, a p53 target gene encoding a cyclin-dependent kinase inhibitor (16, 24, 65), was tested. About a 5.8-fold increase of the p21 protein was detected after Cl-amidine treatment (Fig. 2B). To test whether the increase of p21 is due to the increase of p21 transcription, RT-PCR experiments were performed and an increase of p21 mRNA was detected after the treatment of U2OS cells with Cl-amidine for 24 h (see Fig. S1A in the supplemental material). Thus, Cl-amidine may inhibit cell growth by activating the p53 target genes. To test whether p21 induction by Cl-amidine is dependent on p53, RT-PCR experiments were performed in the $p53^{-/-}$ lung carcinoma cell line H1299. In the absence of p53, the p21 mRNA was undetectable before and after Cl-amidine treatment in H1299 cells (see Fig. S1B in the supplemental material). Further, the expression levels of PAD4 in U2OS cells and H1299 cells were comparable (see Fig. S1C in the supplemental material).

Since p53 is important in the expression of p21, we also examined the level of p53 proteins. Intriguingly, treatment with Cl-amidine increased the amount of the p53 protein in U2OS cells (Fig. 2B). Various genotoxic and nongenotoxic stresses stabilize p53 and often lead to the phosphorylation of multiple serine sites in p53, including the Ser15 site, by ATR, ATM, and extracellular signal-regulated kinases (8, 51). To test whether Cl-amidine treatment imposed a stress leading to the activation of p53, the phosphorylation of p53 at Ser15 was tested. An increase of p53 Ser15 phosphorylation in parallel with the increase of p53 was detected (Fig. 2B), suggesting that the increase of p53 Ser15 phosphorylation may be a result of the increase in the total p53 or the activity of an upstream kinase.

To further test whether the induction of p21 by Cl-amidine depends on p53, we first depleted p53 by shRNA in U2OS cells. The knockdown of p53 by the pHTP/p53-shRNA plasmid was confirmed by Western blotting (Fig. 2C). After treatment of cells with Cl-amidine, p21 expression was increased ~4-fold (4.0- ± 0.18-fold, n = 3) in cells transfected with a control pHTP plasmid (Fig. 2C, lanes 1 and 2) but not in cells after p53

depletion (Fig. 2C, lanes 3 and 4). We also examined the induction of p21 by Cl-amidine in the isogenic $p53^{+/+}$ and $p53^{-/-}$ colorectal carcinoma HCT116 cells, which express similar amounts of PAD4 but differ in their p53 expression (see Fig. S1D in the supplemental material). Western blotting showed that p21 expression was increased by 7.7- ± 1.3-fold (n = 3) in the $p53^{+/+}$ HCT116 cells (Fig. 2D, lanes 1 and 2) but not in the $p53^{-/-}$ HCT116 cells (Fig. 2D, lanes 3 and 4), suggesting that the activation of p21 by Cl-amidine is p53 dependent. The lower PAD4 band of the PAD4 doublets in the HCT116 cells was not visualized at short exposure. Also noted is that the amount of p53 was not significantly increased in the HCT116 $p53^{+/+}$ cells after Cl-amidine treatment (Fig. 2D). To test whether Cl-amidine treatment can increase p21 expression in other cancer cell lines, we tested MCF-7 cells, in which the expression of PAD4 is inducible by estrogen (14, 15). Cl-amidine treatment activated the expression of p21 in the $p53^{+/+}$ MCF-7 cells without elevating the amount of p53 (see Fig. S1E in the supplemental material). Taken together, these results suggest that the inhibition of PAD4 can lead to the increase of p21 expression in a p53-dependent manner.

Depletion of PAD4 increased the expression of a subset of p53 target genes and apoptosis. To inhibit PAD4 functions using an alternative method, we depleted PAD4 from U2OS cells by RNA interference. PAD4 siRNA treatment caused an ~60% decrease in PAD4 and an ~6-fold increase in p21 protein relative to that of the control siRNA treatment (Fig. 3A), suggesting that PAD4 negatively regulates the expression of p21 in U2OS cells. To analyze whether p53 depletion affects other p53 target genes, RT-PCR experiments were performed. Depletion of PAD4 in U2OS cells had essentially no effect on transcription of MDM2 and CDC25C, target genes directly repressed by p53 (38) (Fig. 3B). In contrast, GADD45, PUMA, and p21 exhibited approximately a twofold increase in expression (Fig. 3B), suggesting that the depletion of PAD4 activates a subset of p53 target genes. To test whether the increase in p21 expression by PAD4 depletion is p53 dependent, PAD4 siRNA treatment was performed in U2OS cells with stable transfection of the p53-shRNA plasmid or with the control pHTP plasmid. We found that the depletion of PAD4 by siRNA increased the expression of p21 by 4.5- ± 0.4-fold (n = 3) in the cells transfected with the pHTP plasmid (Fig. 3C, lanes 1 and 2) but not in cells with p53 depletion (Fig. 3C, lanes 3 and 4). These results indicate that the increase in p21 expression after PAD4 depletion in U2OS cells is p53 dependent.

The RT-PCR analyses showed that the depletion of PAD4 increased the expression of certain p53 target genes regulating cell cycle progression and apoptosis. In agreement with the gene expression results, we found that the number of U2OS cells treated with the PAD4 siRNAs was 52.3% ± 4.3% (n = 3) of that of the GFP siRNA-treated cells (Fig. 3D), suggesting a decrease in cell growth or an increase in cell apoptosis after PAD4 siRNA treatment. To detect whether PAD4 siRNA treatment led to apoptosis, we carried out fluorometric TUNEL analyses and found that 25.3% ± 3.1% (52/205, n = 3) of U2OS cell were TUNEL positive after 60 h of treatment with PAD4 siRNAs. In contrast, only ~1.6% (4/244) of U2OS cells treated with the GFP siRNAs were TUNEL positive. To analyze the relationship of PAD4 with apoptosis, we performed staining with the PAD4 antibody, TUNEL, and the DNA dye Hoechst stain. After the GFP siRNA treatment, each cell had a comparable amount of PAD4, and TUNEL-positive cells were rarely detected (Fig. 3E, a to c). In contrast, after the PAD4 siRNA treatment, cells with decreased PAD4 were positively stained by TUNEL (Fig. 3E, d to f). Another set of representative images of the PAD4, TUNEL, and Hoechst staining of U2OS cells after PAD4 siRNA treatment

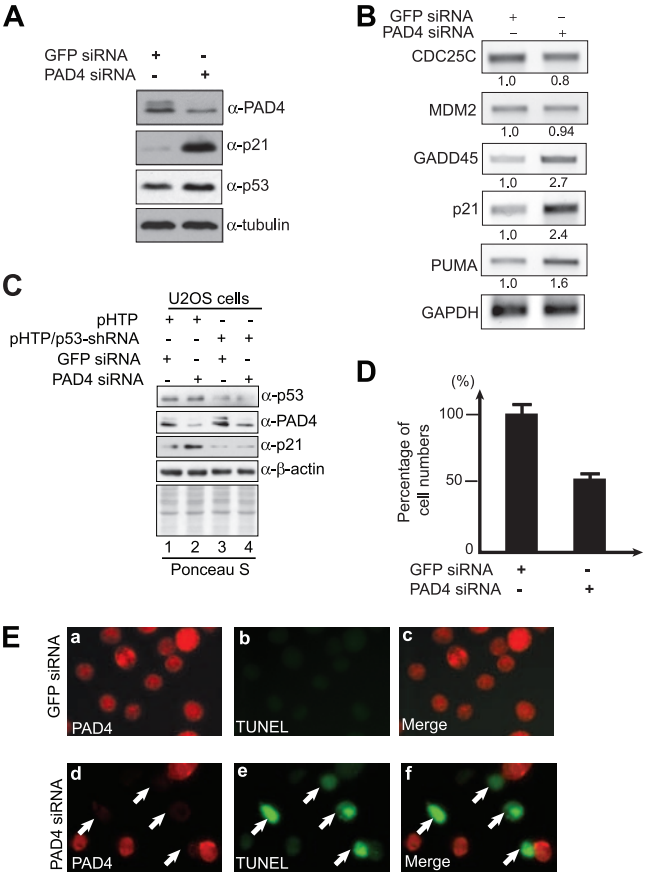

FIG. 3. Effect of PAD4 depletion by siRNAs on the expression of p53 target genes and apoptosis in U2OS cells. (A) PAD4 protein was decreased in U2OS cells after the PAD4 siRNA treatment compared to that after the GFP siRNA treatment. Note the doublet of PAD4 in U2OS cells. PAD4 siRNA caused the PAD4 protein level to decrease ~60%. An approximately sixfold increase in p21 was observed. Tubulin blotting showed equal protein loading. (B) The levels of GADD45, p21, and PUMA mRNAs were increased in U2OS cells after the PAD4 siRNA treatment over that in the cells treated with the GFP siRNA. In contrast, the levels of other p53 target genes, such as CDC25C and MDM2, were unchanged. (C) Effect of PAD4 depletion by siRNAs on the expression of p21 in U2OS cells without or with the depletion of p53 using a pHTP/p53-shRNA plasmid. (D) Cells were treated with the PAD4 siRNAs or the GFP siRNA as a control for 60 h. The number of PAD4 siRNA-treated cells was 52.3% ± 4.3% (n = 3) of that of the GFP siRNA-treated cells, suggesting that PAD4 depletion inhibits cell growth and proliferation. (E) PAD4 staining and TUNEL staining in cells treated with GFP siRNAs (a to c) or PAD4 siRNAs (d to f). Approximately equal amounts of PAD4 were detected in all cells after the GFP siRNA treatment (a). In contrast, a large fraction of cells in subpanel d exhibited little or no PAD4 staining following PAD4 siRNA treatment (denoted by arrows); TUNEL-positive cells were detected in PAD4 siRNA-treated cells (e) but not in the GFP siRNA-treated cells (b); in the merged images (f), cells with decreased PAD4 were found to be TUNEL positive.

is shown in Fig. S2 in the supplemental material. These results indicate a correlation between the decrease in PAD4 and the increase in apoptosis.

Depletion of PAD4 induced the expression of p21, apoptosis, and cell cycle arrest in a p53-dependent manner in HCT116 cells. The p21 gene has served as a model for studying gene regulation by p53 (4, 17, 18, 29, 58). In the rest of this report, we used the p21 gene as a model to characterize the role of PAD4 in gene regulation. To test whether the increase of p21 expression by PAD4 depletion is p53 dependent in the isogenic $p53^{+/+}$ and $p53^{-/-}$ HCT116 cells, we transfected these cells with the pHTP or the pHTP/PAD4-shRNA plasmid. The depletion of PAD4 by the PAD4 shRNA was confirmed by Western blotting (Fig. 4A). Compared to cells treated with the pHTP plasmid, Western blotting showed that PAD4 depletion increased the expression of p21 by 2.3- ± 0.3-fold ($n = 3$) in the $p53^{+/+}$ HCT116 cells (Fig. 4A, lanes 1 and 2) but not in the $p53^{-/-}$ HCT116 cells (Fig. 4A, lanes 3 and 4). This increase in p21 protein was accompanied by a 2.5- ± 0.4-fold ($n = 3$) increase in the p21 mRNA in the $p53^{+/+}$ HCT116 cells (Fig. 4B). These results suggest that the increase in p21 expression after PAD4 depletion is p53 dependent in HCT116 cells.

To test whether the apoptosis caused by PAD4 depletion was p53 dependent, flow cytometry experiments were performed. After the transfection of PAD4 shRNA and puromycin selection for 6 days, we found that the percentage of apoptotic cells was increased to 47.4% ± 1.8% ($n = 3$) in the $p53^{+/+}$ HCT116 cells transfected with the PAD4 shRNA (Fig. 4C, column 2) compared to 23.3% ± 3.8% ($n = 3$) apoptotic cells in the $p53^{+/+}$ HCT116 cells transfected with the pHTP vector (Fig. 4C, column 1). The percentage of apoptotic cells was not significantly increased in the $p53^{-/-}$ HCT116 cells transfected with the PAD4 shRNA compared to cells transfected with the pHTP vector (Fig. 4C, compare columns 3 and 4). These results show that PAD4 depletion increased the percentage of apoptotic cells in a p53-dependent manner in HCT116 cells. The high levels of apoptotic cells after the pHTP vector transfection in both $p53^{+/+}$ and $p53^{-/-}$ HCT116 cells were likely due to the puromycin treatment, which kills untransfected cells.

p53 target genes, such as p21, are involved in the regulation of the cell cycle progression (24, 65). The increase in the expression of p21, a cell cycle inhibitor, prompted us to analyze the cell cycle progression after PAD4 depletion. Flow cytometry analyses showed that the depletion of PAD4 by shRNA increased the population of G_1 cells with a concomitant decrease of the S and G_2/M cells in the $p53^{+/+}$ HCT116 cells (Fig. 4D, top panels) but not in the $p53^{-/-}$ HCT116 cells (Fig. 4D, bottom panels), suggesting that the depletion of PAD4 caused a G_1 cell cycle block in a p53-dependent manner.

Interaction of PAD4 and p53 provides a mechanism for promoter targeting of PAD4. p53 is known to recruit corepressors, such as HDAC1 and HDAC2, to regulate gene expression (22, 27, 29, 37, 38). Because PAD4 has no distinguishable motif for DNA binding and the inhibition of PAD4 increased p21 expression, we postulated that PAD4 might be targeted to specific gene promoters by transcription factors, such as p53, to modify histones. To test this idea, we first established a Flag-HA-PAD4 (FH-PAD4)-expressing 293T cell line to analyze the possible interaction between PAD4 and p53. We found that p53 was retained by the α-Flag M2 agarose beads from 293T cells expressing FH-PAD4 but not from 293T cells without FH-PAD4 expression (Fig. 5A). Lanes 1 to 4 had 5, 2.5, 1.25, and 0.625% of the input protein samples, respectively. To further test if endogenous PAD4 and p53 interact, we performed coimmunoprecipitation experiments and found that PAD4 was coimmunoprecipitated from 293T nuclear extracts by a p53 monoclonal antibody but not by the normal mouse immunoglobulin G (IgG) (Fig. 5B). Since a PAD4-interacting protein, the simian virus 40 T antigen, is present in the 293T cells, we also performed coimmunoprecipitation experiments in 293 nuclear extracts and found that p53 was coimmunoprecipitated by the PAD4 antibody but not by the normal rabbit IgG (see Fig. S3A in the supplemental material).

Structural studies showed that PAD4 has two N-terminal immunoglobulin-like domains (IgL1 and IgL2) and a C-terminal catalytic domain (2) (illustrated in Fig. 5C). To test the domain of PAD4 interacting with p53, we generated constructs expressing GST-PAD4 and its derivatives, GST-$PAD4^{IgL1}$ and GST-$PAD4^{IgL1\&2}$ (Fig. 5C). GST fusion proteins expressed and purified from *E. coli* (see Fig. S3B in the supplemental material) were used in GST pull-down experiments. Both GST-PAD4 and GST-$PAD4^{IgL1\&2}$ but not GST-$PAD4^{IgL1}$ was able to pull down p53 from 293T nuclear extracts (Fig. 5D), suggesting that the two immunoglobulin-like domains of PAD4 were sufficient to mediate the interaction of PAD4 and p53, while the IgL1 domain alone was not.

p53 has an N-terminal activation domain, a middle DNA binding domain, and a C-terminal regulatory domain (34) (illustrated in Fig. 5E). To map the region of p53 important for its interaction with PAD4, we prepared GST-p53 full-length, GST-$p53^{1–300}$, and GST-$p53^{301–393}$ fusion proteins (see Fig. S3C in the supplemental material). After incubating the GST fusion protein beads with HA-PAD4 expressed in 293T cells, we found that GST-p53 full length and GST-$p53^{301–393}$ retained PAD4 but GST-$p53^{1–300}$ did not (Fig. 5F). Together, the above GST pull-down experiments showed that the C-terminal regulatory domain of p53 interacts with the N-terminal immunoglobulin-like domains of PAD4 (illustrated in Fig. 5G).

To test whether p53 and PAD4 directly interact, His6-Flag-p53 and GST-PAD4 expressed and purified from *E. coli* (see Fig. S3D and S3E in the supplemental material) were used in pull-down experiments. We found that GST-PAD4 agarose beads retained the His6-Flag-p53 fusion protein (Fig. 5H), suggesting that PAD4 and p53 can interact directly. Taken together, the above protein-protein interaction studies suggest that p53 could target PAD4 to gene promoters.

Dynamic changes in PAD4 association and histone Arg modifications at the p21 promoter following UV irradiation. After genotoxic stress, such as UV irradiation, p53 is stabilized and transported to the nucleus to activate downstream target genes, such as p21 (18, 37, 59). The induction of p21 as well as the binding of p53 and Pol II to the p21 promoter after UVC treatment in U2OS cells was documented previously (18). Further, the activation of the p21 promoter was fast and transient, occurring within the first 2 h after UVC treatment (18). We used this established model system to investigate histone Arg modifications and PAD4 functions at the p21 promoter at different time points after UV irradiation by ChIP analyses in U2OS cells.

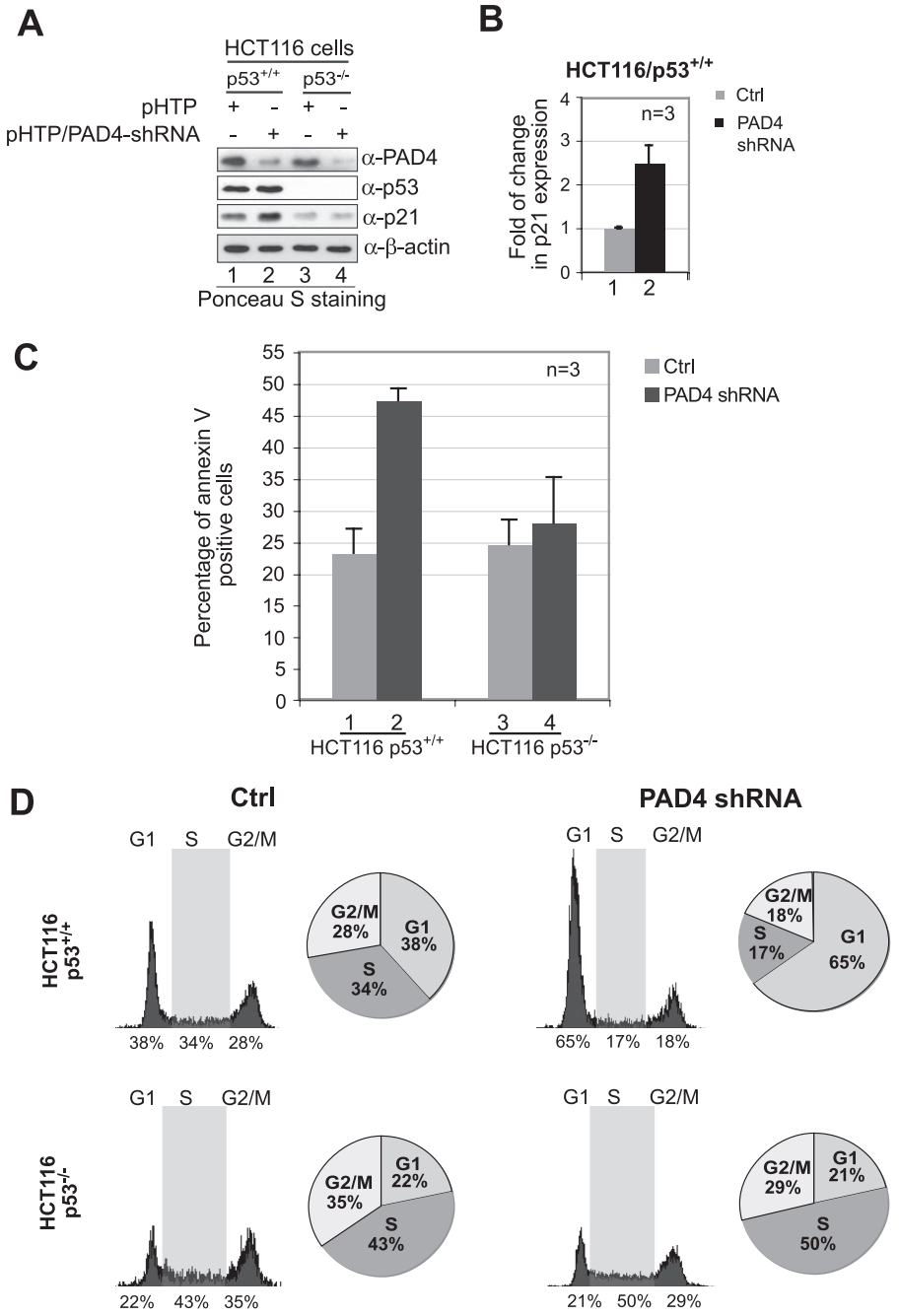

FIG. 4. Depletion of PAD4 increased p21 expression, apoptosis, and cell cycle arrest in a p53-dependent manner in HCT116 cells. (A) Lanes 1 and 2: the changes of PAD4, p21, and p53 proteins after PAD4 depletion by shRNA in the $p53^{+/+}$ HCT116 cells were detected by Western blotting. The expression of p21 was increased by 2.3- ± 0.3-fold ($n = 3$). Lanes 3 and 4: an increase in p21 expression was not detected after PAD4 depletion in the $p53^{-/-}$ HCT116 cells. (B) The expression of p21 was analyzed by RT-PCR experiments. Depletion of PAD4 by the PAD4 shRNA increased the p21 expression in the $p53^{+/+}$ HCT116 cells. (C) The percentages of annexin V-positive cells were analyzed by flow cytometry in the $p53^{+/+}$ and $p53^{-/-}$ HCT116 cells after transfection with the pHTP vector (control) or the PAD4-shRNA and selection with puromycin for 6 days. (D) Flow cytometry analyses of the effects of the PAD4 shRNA treatment on cell cycle progression in the $p53^{+/+}$ and $p53^{-/-}$ HCT116 cells. Ctrl, control.

The p21 promoter has two p53 binding sites, p53BS1 and p53BS2 (Fig. 6A). Before UV treatment, a low amount of p53 was detected on p53 binding site 2 of the p21 gene, which gradually increased following UV irradiation (Fig. 6B). In contrast, PAD4 was detected at the 0-h time point and then decreased at 0.5- and 1-h time points and increased at 2- and 6-h time points following UV irradiation. Western blotting showed that the amount of p53 increased while the amount of PAD4 remained constant after UVC treatment (see Fig. S4A in the supplemental material), suggesting that the disassociation of PAD4 at 0.5- and 1-h time points was not caused by the decrease in PAD4. As a control, we found that p53 and PAD4 were not recruited to the housekeeping gene GAPDH promoter before and after UV irradiation (Fig. 6C), suggesting a

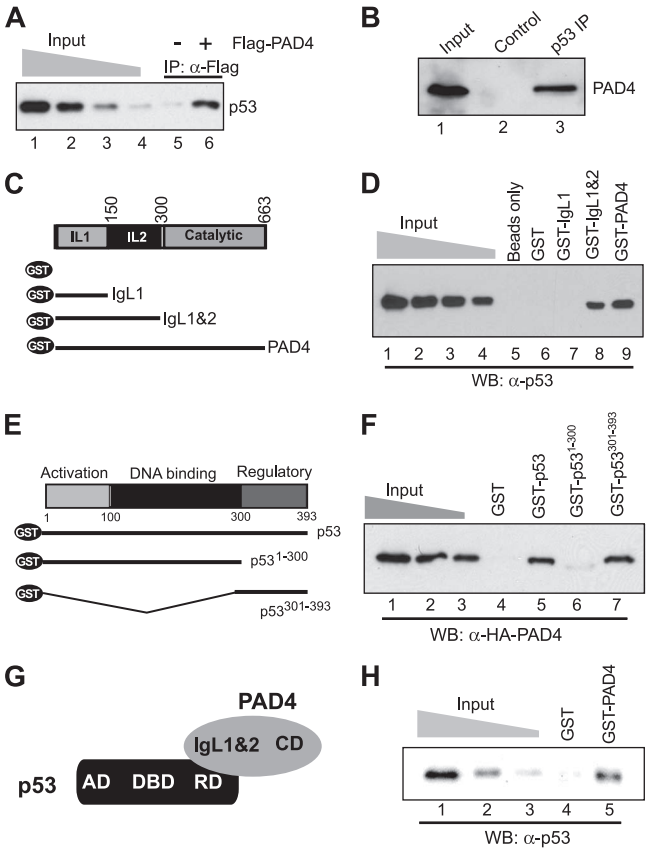

FIG. 5. Interaction of PAD4 and p53. (A) p53 was coimmunoprecipitated by the M2 agarose beads from the Flag-PAD4-expressing 293T cells (lane 6) but not from the parental cells lacking Flag-PAD4 (lane 5). Lanes 1 to 4 had 5, 2.5, 1.25, and 0.625% of input, respectively. (B) Coimmunoprecipitation of endogenous PAD4 by a p53 monoclonal antibody (lane 3) but not by control mouse IgG (lane 2). Lane 1 had 2.5% of the input. (C) Schematic drawing of GST-PAD4 and its derivatives used in the pull-down experiments. (D) p53 was pulled down by GST-PAD4 and GST-PAD4$^{IgL1\&2}$ (lanes 8 and 9), but not GST, GST-PAD4^{IgL1}, or beads alone. Lanes 1 to 4 had 5, 2.5, 1.25, and 0.625% of input, respectively. (E) Illustration of GST-p53 and its derivatives used in the pull-down experiments. (F) GST-p53 (lane 5) and GST-p53$^{301–393}$ (lane 7), but not GST-p53$^{1–300}$ or beads alone, were efficient in mediating the p53 and PAD4 interaction. Lanes 1 to 3 had 2, 1, and 0.5% of the input, respectively. (G) GST pull-down experiments suggest that the N-terminal immunoglobulin-like domains of PAD4 interact with the C-terminal regulatory domain of p53. (H) GST-PAD4 bound to the glutathione agarose beads associated with Flag-His6-p53, suggesting a direct interaction of p53 and PAD4. Lanes 1 to 3 had 5, 2.5, and 1.25% of input, respectively.

gene-specific association of these factors with the p21 promoter. Given that p21 was quickly and transiently expressed after UVC treatment (18), we postulated that the disassociation of PAD4 at the 0.5- and 1-h time points might allow the expression of p21.

To test whether histone citrullination occurs at the p21 promoter, we carried out ChIP experiments using an antibody against citrullinated histone H3 (H3Cit), which was made against a histone H3 peptide (residues 1 to 20) containing citrulline at positions 2, 8, and 17 (14). Histone H3 citrullination at p53 binding site 2 was detected before UV irradiation (Fig. 6B), suggesting that PAD4 is active on the p21 promoter in U2OS cells before exposure to genotoxic stress. Following UV irradiation, we detected a decrease in histone H3 citrullination at 0.5 and 1 h followed by an increase at 2- and 6-h time points (Fig. 6B). This decrease in histone citrullination correlated temporally with the decrease in PAD4 on the promoter. In contrast, histone H3R17 methylation first increased (0.5 and 1 h) and then decreased (2 and 6 h) after UV irradiation. Thus, there is an inverse correlation between the amount of histone H3R17 methylation and the amount of H3 citrullination at the p21 gene promoter following UV irradiation.

To better quantify changes in histone H3 citrullination and Arg methylation as well as PAD4, we performed Q-PCR assays of the ChIP samples. Consistent with the results in Fig. 6B, H3Cit was decreased at 1 h and then increased at 6 h on both p53 binding site 1 and site 2 after UVC treatment (Fig. 6D and F), while H3R17 methylation was first increased at 1 h and then decreased at the 6-h time point (Fig. 6D and F). An initial decrease of PAD4 at 1 h followed by an increase at 6 h on both p53 binding sites was also detected by Q-PCR (Fig. 6D and F). To analyze whether PAD4 preferentially associates with the p53 binding sites, we performed Q-PCR to analyze the association of PAD4 with the +182-bp region of p21. Consistent with a role for p53 in the recruitment of PAD4, the amount of PAD4 at the p53 binding sites was much higher than that at the +182-bp region (see Fig. S4B in the supplemental material).

To monitor whether the nucleosome density at the p53 binding sites changes after UV irradiation, we performed ChIP assays with a histone H3 antibody and found that histone H3 was decreased at both p53 binding sites with different kinetics (see Fig. S4C and S4D in the supplemental material), suggesting that histone octamers were repositioned or evicted from the p53 binding sites after UVC treatment. To reflect changes in H3, H3 citrullination and H3R17 methylation results were normalized to the total amount of histone H3 (Fig. 6E and G). Although the relative values were altered, the trend of changes in H3 citrullination and H3R17 methylation was similar to that before normalization.

PAD4 is recruited to the p21 promoter in a p53-dependent manner. To test whether p53 mediates the recruitment of PAD4 to the p21 promoter, we first performed ChIP experiments in p53$^{-/-}$ H1299 cells with or without the transfection of a p53-expressing plasmid. The expression of p53 was confirmed by Western blotting (Fig. 7A). The association of PAD4 with p53 binding site 2 of the p21 promoter was not detected in cells without p53 expression (Fig. 7B, upper panel) but was detected in cells with p53 expression (Fig. 7B, middle panel). As a control, we found that neither p53 nor PAD4 was detected on the GAPDH gene promoter (Fig. 7B, bottom panel). These results indicate that expression of p53 in the p53$^{-/-}$ H1299 cells is sufficient to recruit PAD4 to the p21 promoter.

To further analyze whether the dynamic association of PAD4 with the p21 promoter after UV irradiation is p53 dependent, we performed ChIP assays in U2OS cells without or with p53 depletion using the cell lines as described for Fig. 2C and 3C. In the stable U2OS cell line transfected with the control pHTP plasmid, p53 gradually accumulated at p53 binding sites 1 and 2 (Fig. 7C and 7E, columns 1 to 3), while much less p53 was detected at these sites after p53 depletion (Fig. 7C and 7E, columns 4 to 6). Dynamic PAD4 association with p53 binding sites 1 and 2 was detected in cells without p53 deple-

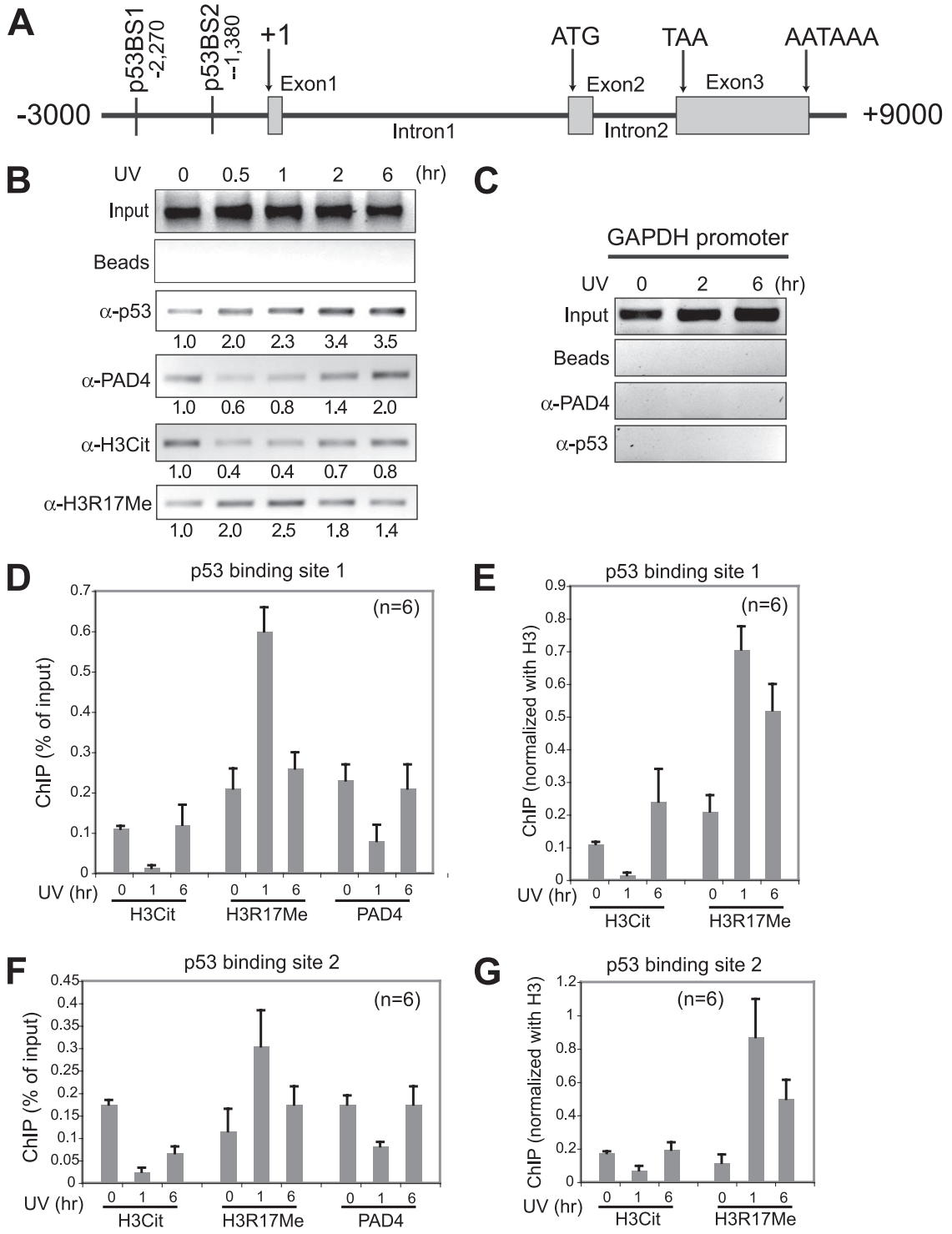

FIG. 6. Dynamic p53 and PAD4 association and histone Arg modifications at the p21 promoter after UV irradiation. (A) Illustration of the p21 gene promoter, including the two p53 binding sites (p53BS1 and p53BS2). (B) Representative ChIP results of p53 and PAD4 association as well as histone Arg modifications at the p53BS2 region of the p21 promoter after 50-J/m^2 UVC irradiation. (C) PAD4 and p53 were not associated with the GAPDH promoter before and after DNA damage treatment. (D) Q-PCR analyses of the H3Cit, H3R17Me, and PAD4 levels on p53 binding site 1 in the U2OS cells at different time points (0, 1, and 6 h) after UVC treatment ($n = 6$). (E) The H3Cit and H3R17Me ChIP results in panel D were normalized to those of histone H3. (F) Q-PCR analyses of the H3Cit, H3R17Me, and PAD4 levels on p53 binding site 2 in the U2OS cells at different time points (0, 1, and 6 h) after UVC treatment ($n = 6$). (G) The H3Cit and H3R17Me ChIP results in panel F were normalized to those of histone H3.

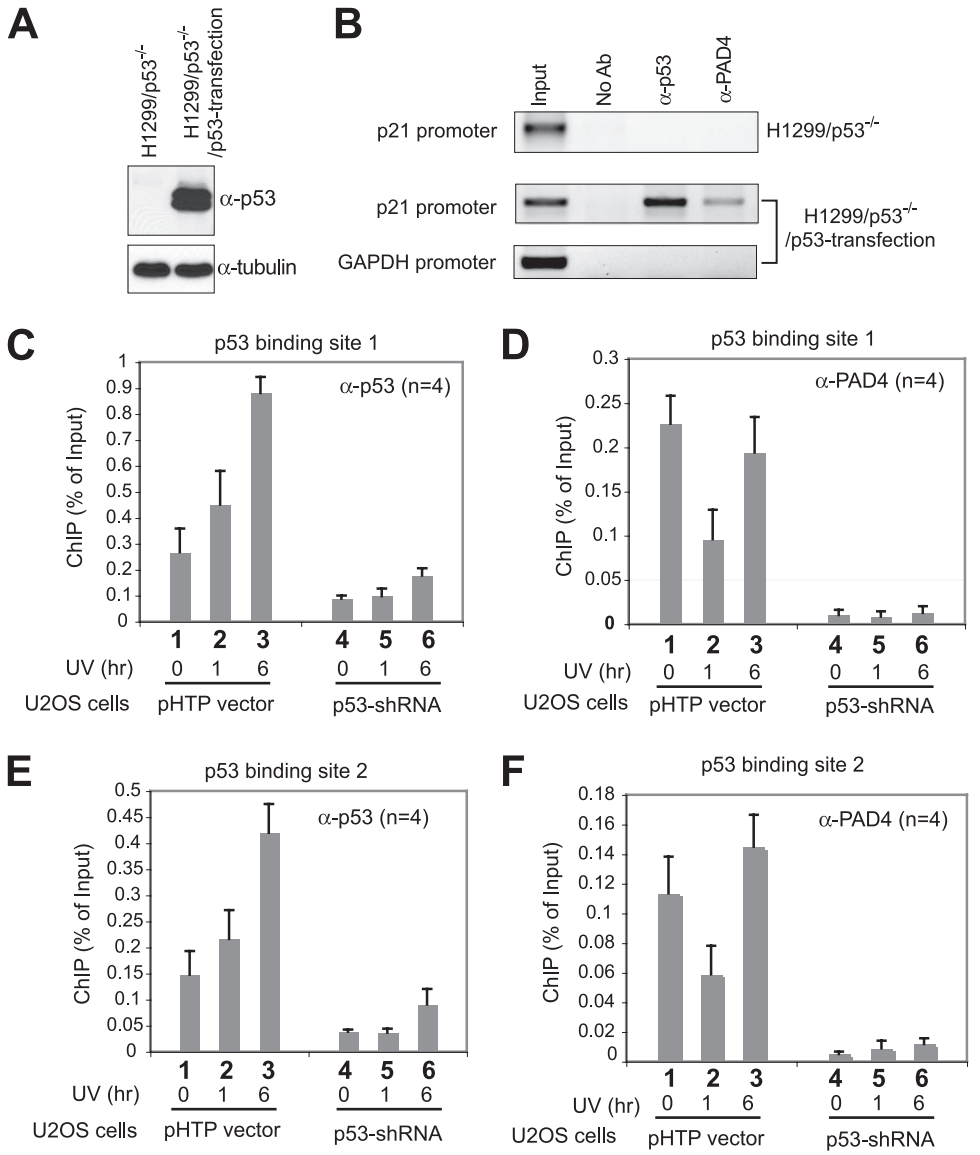

FIG. 7. Association of PAD4 with the p21 promoter is p53 dependent. (A) The expression of p53 in the $p53^{-/-}$ H1299 cells was restored by transient transfection of a p53-expressing plasmid. (B) ChIP analyses of the p53 and PAD4 association with p53 binding site 2 of the p21 promoter in H1299 cells with or without the transfection of a p53-expressing plasmid. (C and D) ChIP assays of p53 (C) or PAD4 (D) association with p53 binding site 1 using Q-PCR in U2OS cells without or with the depletion of p53 by shRNA. (E and F) ChIP assays of p53 (E) or PAD4 (F) association with p53 binding site 2 using Q-PCR in U2OS cells without or with the depletion of p53 by shRNA.

tion by shRNA (Fig. 7D and 7F, columns 1 to 3). In contrast, after p53 depletion, the amount of PAD4 at the p53 binding sites was dramatically decreased (Fig. 7D and 7F, columns 4 to 6), indicating that the association of PAD4 with the p21 promoter is p53 dependent. Taken together, these results support the hypothesis that p53 facilitates PAD4 recruitment to the p21 promoter.

Detection of paused and elongating RNA Pol II by ChIP and permanganate footprinting. The C-terminal domain (CTD) of the largest subunit of human RNA Pol II is composed of 52 repeats of a heptad sequence (YSPTSPS) and becomes phosphorylated on Ser5 during transcriptional initiation (50, 56). To relate the changes in histone modifications to the recruitment of the basal transcriptional machinery, we analyzed the recruitment of RNA Pol II to the p21 promoter. ChIP analyses using a monoclonal antibody (8WG16) against unmodified Pol II CTD showed that Pol II was present at the +182 region of p21 before UV irradiation (Fig. 8A) and was increased at 1 h and then decreased ~10-fold at the 6-h time point (Fig. 8A). These kinetic changes suggest that Pol II is associated with the p21 promoter before UV irradiation in a repressed state and that an additional mechanism of repression occurs 6 h after UV treatment, leading to the loss of Pol II. The phosphorylation of Ser5 of Pol II CTD has been detected on Pol II in close proximity to the transcription start site of active genes or genes with paused RNA Pol II (18, 50, 56). ChIP with an antibody that recognizes the CTD phosphorylated on Ser5 revealed an increase in Pol II Ser5 phosphorylation up to 1 h after UV

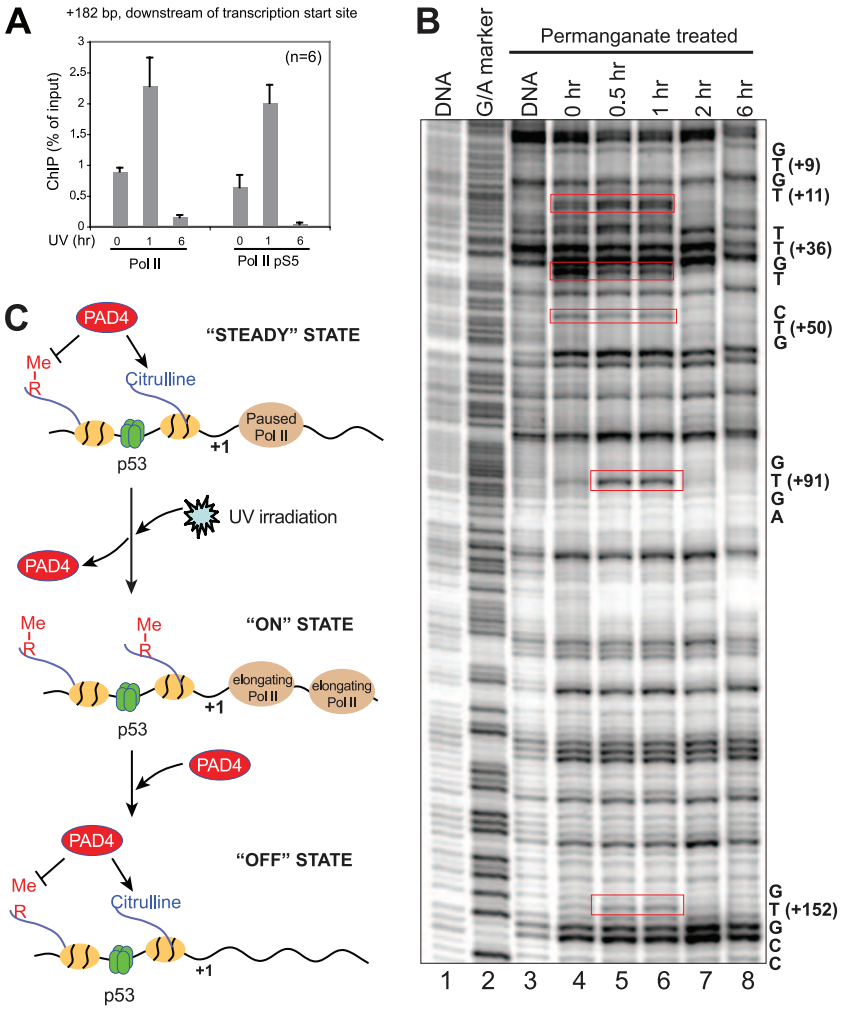

FIG. 8. Detection of paused and elongating RNA Pol II at the p21 promoter. (A) The association of RNA Pol II and Ser5 phosphorylated RNA Pol II was monitored at the +182 region of p21 at different time points after UVC treatment. (B) Permanganate footprinting was used to monitor RNA Pol II at the p21 promoter region during induction by UVC irradiation. Lane 1 shows a background pattern of bands that accompanied the LM-PCR procedure when DNA was not treated with permanganate. Lane 2 shows markers produced by partial cleavage of DNA at purines (G/A). Lane 3 shows permanganate reactivity that was intrinsic to naked DNA. Despite a high background, one can readily detect permanganate-hyperreactive positions at T9, T11, T36, T38, and T50 that occur in cells (lane 4) but not in naked DNA (lane 3). These reactivities were indicative of paused Pol II. Within 30 min after a brief pulse of UV light, permanganate reactivities at T91 and T152 increased and provided evidence of Pol II undergoing productive elongation at 0.5 and 1 h after UV treatment. By 2 and 6 h, transcription appeared repressed since the permanganate reactivity marking paused and elongating forms of Pol II had decreased significantly. (C) A "three-state" model for the role of PAD4 and dynamic histone Arg modifications in the expression of the p21 gene after UV irradiation (see text for further details).

irradiation followed by a dramatic decrease at 6 h (Fig. 8A). These ChIP data with Pol II antibodies are in agreement with previously reported observations (18).

The association of RNA Pol II and the Ser5 phosphorylation of RNA Pol II CTD suggests that RNA Pol II might be paused at this promoter before UV irradiation. To obtain more insight into the behavior of Pol II at the p21 promoter in response to UV irradiation, we performed permanganate footprinting. Permanganate preferentially reacts with thymines (T's) in transcription bubbles associated with RNA Pol II engaged in transcription, thereby detecting both paused and elongating Pol II (9). This technique detects transcriptionally engaged Pol II and maps the locations of these Pol II molecules with a resolution of about 15 bp and is thereby an ideal method to monitor transcriptional activity of Pol II following gene activation.

Permanganate footprinting analyses of U2OS cells before UV irradiation detected hyperreactive thymines at positions 9, 11, 36, 38, and 50 of p21 (Fig. 8B, lane 4), suggesting that Pol II is paused in this region. At 30 min and 1 h after UV treatment, we observed increases in the permanganate reactivity at positions 91 and 152, indicating active transcription (Fig. 8B, lanes 5 and 6). The permanganate reactivity that persisted in the region proximal to the transcription start site (e.g., +9, +11, etc.) probably reflects reinitiation by Pol II and transient pausing as previously seen on the hsp70 heat shock gene (48). Interestingly, there were significant changes in the permanganate reactivity from the 1-h to the 2-h time point following UV irradiation. The permanganate reactivity at +91 and +152 decreased (Fig. 8B, lanes 7 and 8), suggesting that active transcription had stopped. Even more intriguing, the permanga-

nate reactivity in the promoter-proximal region vanished, suggesting that the association of Pol II with the p21 promoter becomes blocked.

Our permanganate footprinting results fit very well with our ChIP data. The Pol II detected by ChIP before UV irradiation could be paused Pol II producing permanganate reactivity in the promoter-proximal region. The increase in Pol II detected by ChIP within 1 h of UV irradiation corresponded to Pol II molecules undergoing active elongation and reinitiation as indicated by the increased permanganate reactivity downstream from the promoter-proximal region. Finally, at the 6-h time points, both assays showed a decrease in Pol II below the level observed prior to UV treatment.

DISCUSSION

In this study, we provide evidence that PAD4 is recruited by p53 to the p21 gene to repress transcription. This conclusion is based on several independent types of experiments. Inactivation of PAD4 with an inhibitor and depletion of PAD4 with siRNA or shRNA both increased the level of p21 transcription. The increase of p21 expression by PAD4 inhibition or depletion was p53 dependent. The results of the siRNA treatment probably underestimate the extent of this increase because immunofluorescence analyses indicate that only a fraction of the cells were depleted of PAD4 by our siRNA protocol. Biochemical assays indicated that p53 interacts with PAD4 both in cells and when combined as purified proteins. ChIP analyses found that the association of PAD4 with the p21 promoter is p53 dependent. Finally, our kinetic analyses of protein association with the p21 promoter following UV induction indicate that PAD4 was associated with p21 when the promoter was repressed but decreased when the promoter was active. The increase in histone Arg methylation and the decrease in histone citrullination occurred when the promoter was active. Conversely, the increase in histone citrullination and the decrease in histone Arg methylation occurred when the promoter was repressed. Interestingly, the permanganate footprinting identified two distinct repressed states. One involved a paused Pol II that was detected in the promoter-proximal region before UV induction. The other was at 2 to 6 h after UV induction when the promoter seemed to shut off due to the absence of Pol II recruitment to the promoter.

Based on the above results, we propose a model in which the expression of p21 is controlled at the "steady," "on," and "off" stages after UVC treatment (see the model in Fig. 8C). (i) In cells without exposure to DNA damage, PAD4 and histone citrullination maintain histone Arg methylation and the transcription of p21 at a low level. RNA Pol II bound to p21 is in a nonproductive and paused state. (ii) Shortly after UV irradiation, histone Arg methylation increases while histone citrullination decreases. These changes in histone Arg modifications correlate with the "on" stage of gene expression. (iii) At a later stage following UV treatment, when the expression of p21 is turned "off," histone citrullination mediated by PAD4 increases with a concomitant decrease of histone Arg methylation and RNA Pol II associated with p21. Two factors, the PAD4 activity and the histone dynamics, could contribute to the decrease in histone Arg methylation.

An et al. have first shown that histone Arg methylation mediated by CARM1 and PRMT1 activates p53-mediated gene expression (1). In this study, we found that PAD4 is involved in repressing the expression of a subset of p53 target genes, including p21, GADD45, and PUMA. We focused on the p21 gene to analyze the kinetics of PAD4 association, histone Arg methylation, and citrullination and relate chromatin events to the RNA Pol II activities at the promoter. Inhibition or depletion of PAD4 increased p21 expression in cells without DNA damage treatment, suggesting that PAD4 is involved in repressing the p21 expression under regular culture conditions. In addition, both histone Arg methylation and citrullination were detected on the p21 promoter before DNA damage, suggesting that a dynamic balance of histone Arg methylation and citrullination is reached by two opposing enzymatic activities mediated by CARM1 and PAD4, respectively.

Dynamic changes of histone Arg methylation and citrullination were detected on the p21 gene promoter after UV irradiation. In particular, a decrease of PAD4 and histone citrullination as well as an increase of histone Arg methylation was temporally correlated with the rapid and transient activation of p21. This quick but brief activation of gene expression has been detected by several different approaches, including RNA fluorescent in situ hybridization (18), permanganate genomic footprinting (this study), and ChIP with the RNA Pol II antibodies (reference 18 and this study). It is unknown what regulates the dissociation of PAD4 from p21 during the "on" stage of gene expression. The C-terminal regulatory domain of p53 is subjected to many posttranslational modifications, including methylation, acetylation, and phosphorylation (8, 13, 21, 28, 37). p53 phosphorylation and acetylation play a role in recruiting protein factors, such as 14-3-3 (63) and p300/CBP (4, 17, 45), respectively. Whether p53 modifications negatively regulate the PAD4 and p53 interaction will be explored in our future experiments.

It is very striking that the amount of RNA Pol II on the p21 promoter decreased dramatically following an initial activation within 2 h after UV treatment. Therefore, under the condition of UV irradiation, there is a decrease in the rate of RNA Pol II reinitiation to repress gene expression. ChIP experiments found that the amount of p53 associated with the p21 promoter remained at a high level even after the decrease of the amount of RNA Pol II, suggesting that the association of p53 with the p21 promoter was not enough to mediate continued transcription. Interestingly, PAD4 and histone citrullination were detected at high levels around the time points when RNA Pol II reinitiation was decreased. It is possible that p53 recruits a different set of chromatin-modifying factors, such as PAD4, to the p21 promoter to generate a chromatin structure unfavorable for continuing RNA Pol II recruitment and transcription. It remains unknown whether various stress signals affect the expression of p21 by regulating RNA Pol II recruitment. At least, under the condition of stalled DNA replication after hydroxyurea treatment, the lack of p21 induction was found to be due to the decrease of Pol II elongation (44). Thus, the p21 gene expression can be regulated at multiple steps of the transcription cycle, including initiation and elongation.

The expression of PAD4 in MCF-7 cells is induced by estrogen (14, 15), a hormone that increases the cell growth rate. On the other hand, PAD4 is highly expressed in HL-60

cells after retinoic acid treatment (46), which induces the terminal differentiation of HL-60 cells along the granulocyte lineage, suggesting that PAD4 may play a unique role in granulocytes/neutrophils. However, whether PAD4 plays cell-specific roles in cell growth or differentiation is unclear. Our studies showed that PAD4 might facilitate cell growth by repressing the p53 target genes in MCF-7, U2OS, and HCT116 cells. This would be consistent with a report showing that PAD4 is overexpressed in multiple human cancers (10). On the other hand, a recent report showed that the overexpression of PAD4 eventually led to apoptosis of both HL-60 and Jurkat cells (41), suggesting that PAD4 has a proapoptotic role in the hematopoietic cells. It was also reported that the overexpression of PAD4 in Jurkat cells increased the amounts of p53 and p21 and induced apoptosis (41). However, p53 in Jurkat cells carries multiple point mutations (12), and Jurkat cells did not respond to DNA-damaging drugs to express p21 (26, 43). Further, Jurkat cells did not respond to gamma irradiation to stabilize p53 (53). Together, these reports suggest that Jurkat cells do not have a functioning p53 pathway. Because Liu et al. reported that PAD4 can induce apoptosis also in HL-60 cells (41), which are $p53^{-/-}$, the proapoptotic function of PAD4 is not p53 dependent in HL-60 cells. Our results showed that the Jurkat cells had very low levels of p53 and an undetectable amount of p21 (see Fig. S5A in the supplemental material). When PAD4 was overexpressed in Jurkat cells by transient transfection, the increase of p53 or p21 was not observed (see Fig. S5B in the supplemental material). Further, breast cancer MCF-7 cells stably expressing FH-PAD4 did not show an increase of apoptosis (data not shown). Western blot analyses indicated that the amount of p53 and p21 protein in the Flag-HA-PAD4/MCF7 cells was decreased (see Fig. S5C in the supplemental material), suggesting that PAD4 has a repressive role for p53 in MCF-7 cells. Therefore, the mechanism by which PAD4 overexpression induces apoptosis in hematopoietic cancer cells remains to be further explored.

Our current understanding of the PAD4 and histone citrullination regulation is very limited. Histone citrullination has been detected on the estrogen-responsive pS2 gene promoter (14, 62) and the p21 promoter (this study). The interaction of PAD4 with a particular transcription factor, such as p53, likely increases the local concentration of PAD4 around specific promoters and facilitates its modification of histones to regulate gene expression. On the other hand, global histone citrullination is maintained at a very low level in differentiated HL-60 cells (47, 62) and MCF-7 cells (14). Multiple mechanisms can be proposed for the metabolic destiny of citrulline in histones, including the replacement of citrullinated histones with histone variants and the eviction of nucleosomes during gene expression, as well as enzyme-catalyzed conversion of citrulline to Arg by another yet-to-be-identified protein.

ACKNOWLEDGMENTS

We thank Yali Dou (University of Michigan), Xiaoting Zhang (University of Cincinnati), Yanan Tian (Texas A&M University), and Bert Vogelstein (Johns Hopkins University) for plasmids and cell lines. We thank Franklin Pugh, Joseph Reese, and Song Tan for helpful discussions and Joseph Reese for critical reading of the manuscript. We thank the Center for Quantitative Cell Analysis for flow cytometry analyses and the Nucleic Acid Facility at the Huck Institute of the Life Sciences (Penn State University) for help in DNA sequencing and real-time PCR analyses.

Research in the P.R.T. laboratory is supported by NIH grant GM079357. Research in the laboratory of Y.W. is supported by a startup fund from PSU and a seed grant award from Johnson & Johnson Inc., Penn State University, and TSF.

REFERENCES

1. **An, W., J. Kim, and R. G. Roeder.** 2004. Ordered cooperative functions of PRMT1, p300, and CARM1 in transcriptional activation by p53. Cell **117:** 735–748.
2. **Arita, K., H. Hashimoto, T. Shimizu, K. Nakashima, M. Yamada, and M. Sato.** 2004. Structural basis for Ca^{2+}-induced activation of human PAD4. Nat. Struct. Mol. Biol. **11:**777–783.
3. **Balint, B. L., A. Szanto, A. Madi, U. M. Bauer, P. Gabor, S. Benko, L. G. Puskas, P. J. Davies, and L. Nagy.** 2005. Arginine methylation provides epigenetic transcription memory for retinoid-induced differentiation in myeloid cells. Mol. Cell. Biol. **25:**5648–5663.
4. **Barlev, N. A., L. Liu, N. H. Chehab, K. Mansfield, K. G. Harris, T. D. Halazonetis, and S. L. Berger.** 2001. Acetylation of p53 activates transcription through recruitment of coactivators/histone acetyltransferases. Mol. Cell **8:**1243–1254.
5. **Barski, A., S. Cuddapah, K. Cui, T. Y. Roh, D. E. Schones, Z. Wang, G. Wei, I. Chepelev, and K. Zhao.** 2007. High-resolution profiling of histone methylations in the human genome. Cell **129:**823–837.
6. **Bauer, U. M., S. Daujat, S. J. Nielsen, K. Nightingale, and T. Kouzarides.** 2002. Methylation at arginine 17 of histone H3 is linked to gene activation. EMBO Rep. **3:**39–44.
7. **Berger, S. L.** 2007. The complex language of chromatin regulation during transcription. Nature **447:**407–412.
8. **Brooks, C. L., and W. Gu.** 2003. Ubiquitination, phosphorylation and acetylation: the molecular basis for p53 regulation. Curr. Opin. Cell Biol. **15:** 164–171.
9. **Cartwright, I. L., D. E. Cryderman, D. S. Gilmour, L. A. Pile, L. L. Wallrath, J. A. Weber, and S. C. Elgin.** 1999. Analysis of Drosophila chromatin structure in vivo. Methods Enzymol. **304:**462–496.
10. **Chang, X., and J. Han.** 2006. Expression of peptidylarginine deiminase type 4 (PAD4) in various tumors. Mol. Carcinog. **45:**183–196.
11. **Chen, D., H. Ma, H. Hong, S. S. Koh, S. M. Huang, B. T. Schurter, D. W. Aswad, and M. R. Stallcup.** 1999. Regulation of transcription by a protein methyltransferase. Science **284:**2174–2177.
12. **Cheng, J., and M. Haas.** 1990. Frequent mutations in the p53 tumor suppressor gene in human leukemia T-cell lines. Mol. Cell. Biol. **10:**5502–5509.
13. **Chuikov, S., J. K. Kurash, J. R. Wilson, B. Xiao, N. Justin, G. S. Ivanov, K. McKinney, P. Tempst, C. Prives, S. J. Gamblin, N. A. Barlev, and D. Reinberg.** 2004. Regulation of p53 activity through lysine methylation. Nature **432:**353–360.
14. **Cuthbert, G. L., S. Daujat, A. W. Snowden, H. Erdjument-Bromage, T. Hagiwara, M. Yamada, R. Schneider, P. D. Gregory, P. Tempst, A. J. Bannister, and T. Kouzarides.** 2004. Histone deimination antagonizes arginine methylation. Cell **118:**545–553.
15. **Dong, S., Z. Zhang, and H. Takahara.** 2007. Estrogen-enhanced peptidylarginine deiminase type IV gene (PADI4) expression in MCF-7 cells is mediated by estrogen receptor-alpha-promoted transfactors activator protein-1, nuclear factor-Y, and Sp1. Mol. Endocrinol. **21:**1617–1629.
16. **el-Deiry, W. S., T. Tokino, V. E. Velculescu, D. B. Levy, R. Parsons, J. M. Trent, D. Lin, W. E. Mercer, K. W. Kinzler, and B. Vogelstein.** 1993. WAF1, a potential mediator of p53 tumor suppression. Cell **75:**817–825.
17. **Espinosa, J. M., and B. M. Emerson.** 2001. Transcriptional regulation by p53 through intrinsic DNA/chromatin binding and site-directed cofactor recruitment. Mol. Cell **8:**57–69.
18. **Espinosa, J. M., R. E. Verdun, and B. M. Emerson.** 2003. p53 functions through stress- and promoter-specific recruitment of transcription initiation components before and after DNA damage. Mol. Cell **12:**1015–1027.
19. **Gomes, N. P., G. Bjerke, B. Llorente, S. A. Szostek, B. M. Emerson, and J. M. Espinosa.** 2006. Gene-specific requirement for P-TEFb activity and RNA polymerase II phosphorylation within the p53 transcriptional program. Genes Dev. **20:**601–612.
20. **Gu, W., and R. G. Roeder.** 1997. Activation of p53 sequence-specific DNA binding by acetylation of the p53 C-terminal domain. Cell **90:**595–606.
21. **Gu, W., X. L. Shi, and R. G. Roeder.** 1997. Synergistic activation of transcription by CBP and p53. Nature **387:**819–823.
22. **Gui, C. Y., L. Ngo, W. S. Xu, V. M. Richon, and P. A. Marks.** 2004. Histone deacetylase (HDAC) inhibitor activation of p21WAF1 involves changes in promoter-associated proteins, including HDAC1. Proc. Natl. Acad. Sci. USA **101:**1241–1246.
23. **Harms, K. L., and X. Chen.** 2007. Histone deacetylase 2 modulates p53 transcriptional activities through regulation of p53-DNA binding activity. Cancer Res. **67:**3145–3152.
24. **Harper, J. W., G. R. Adami, N. Wei, K. Keyomarsi, and S. J. Elledge.** 1993.

The p21 Cdk-interacting protein Cip1 is a potent inhibitor of G1 cyclin-dependent kinases. Cell **75:**805–816.
25. **Harris, S. L., and A. J. Levine.** 2005. The p53 pathway: positive and negative feedback loops. Oncogene **24:**2899–2908.
26. **Hellin, A. C., M. Bentires-Alj, M. Verlaet, V. Benoit, J. Gielen, V. Bours, and M. P. Merville.** 2000. Roles of nuclear factor-kappaB, p53, and p21/WAF1 in daunomycin-induced cell cycle arrest and apoptosis. J. Pharmacol. Exp. Ther. **295:**870–878.
27. **Ho, J., and S. Benchimol.** 2003. Transcriptional repression mediated by the p53 tumour suppressor. Cell Death Differ. **10:**404–408.
28. **Huang, J., L. Perez-Burgos, B. J. Placek, R. Sengupta, M. Richter, J. A. Dorsey, S. Kubicek, S. Opravil, T. Jenuwein, and S. L. Berger.** 2006. Repression of p53 activity by Smyd2-mediated methylation. Nature **444:**629–632.
29. **Huang, J., R. Sengupta, A. B. Espejo, M. G. Lee, J. A. Dorsey, M. Richter, S. Opravil, R. Shiekhattar, M. T. Bedford, T. Jenuwein, and S. L. Berger.** 2007. p53 is regulated by the lysine demethylase LSD1. Nature **449:**105–108.
30. **Huang, S., M. Litt, and G. Felsenfeld.** 2005. Methylation of histone H4 by arginine methyltransferase PRMT1 is essential in vivo for many subsequent histone modifications. Genes Dev. **19:**1885–1893.
31. **Jin, Y., Y. Wang, J. Johansen, and K. M. Johansen.** 2000. JIL-1, a chromosomal kinase implicated in regulation of chromatin structure, associates with the male specific lethal (MSL) dosage compensation complex. J. Cell Biol. **149:**1005–1010.
32. **Kelly, W. K., and P. A. Marks.** 2005. Drug insight: histone deacetylase inhibitors—development of the new targeted anticancer agent suberoylanilide hydroxamic acid. Nat. Clin. Pract. Oncol. **2:**150–157.
33. **Khorasanizadeh, S.** 2004. The nucleosome: from genomic organization to genomic regulation. Cell **116:**259–272.
34. **Kitayner, M., H. Rozenberg, N. Kessler, D. Rabinovich, L. Shaulov, T. E. Haran, and Z. Shakked.** 2006. Structural basis of DNA recognition by p53 tetramers. Mol. Cell **22:**741–753.
35. **Klose, R. J., and Y. Zhang.** 2007. Regulation of histone methylation by demethylimination and demethylation. Nat. Rev. Mol. Cell Biol. **8:**307–318.
36. **Kouzarides, T.** 2007. Chromatin modifications and their function. Cell **128:**693–705.
37. **Laptenko, O., and C. Prives.** 2006. Transcriptional regulation by p53: one protein, many possibilities. Cell Death Differ. **13:**951–961.
38. **Le Gac, G., P. O. Esteve, C. Ferec, and S. Pradhan.** 2006. DNA damage-induced down-regulation of human Cdc25C and Cdc2 is mediated by cooperation between p53 and maintenance DNA (cytosine-5) methyltransferase 1. J. Biol. Chem. **281:**24161–24170.
39. **Li, B., M. Carey, and J. L. Workman.** 2007. The role of chromatin during transcription. Cell **128:**707–719.
40. **Li, H., W. Fischle, W. Wang, E. M. Duncan, L. Liang, S. Murakami-Ishibe, C. D. Allis, and D. J. Patel.** 2007. Structural basis for lower lysine methylation state-specific readout by MBT repeats of L3MBTL1 and an engineered PHD finger. Mol. Cell **28:**677–691.
41. **Liu, G. Y., Y. F. Liao, W. H. Chang, C. C. Liu, M. C. Hsieh, P. C. Hsu, G. J. Tsay, and H. C. Hung.** 2006. Overexpression of peptidylarginine deiminase IV features in apoptosis of haematopoietic cells. Apoptosis **11:**183–196.
42. **Luo, Y., K. Arita, M. Bhatia, B. Knuckley, Y. H. Lee, M. R. Stallcup, M. Sato, and P. R. Thompson.** 2006. Inhibitors and inactivators of protein arginine deiminase 4: functional and structural characterization. Biochemistry **45:**11727–11736.
43. **Mansilla, S., B. Pina, and J. Portugal.** 2003. Daunorubicin-induced variations in gene transcription: commitment to proliferation arrest, senescence and apoptosis. Biochem. J. **372:**703–711.
44. **Mattia, M., V. Gottifredi, K. McKinney, and C. Prives.** 2007. p53-dependent p21 mRNA elongation is impaired when DNA replication is stalled. Mol. Cell. Biol. **27:**1309–1320.
45. **Mujtaba, S., Y. He, L. Zeng, S. Yan, O. Plotnikova, Sachchidanand, R. Sanchez, N. J. Zeleznik-Le, Z. Ronai, and M. M. Zhou.** 2004. Structural mechanism of the bromodomain of the coactivator CBP in p53 transcriptional activation. Mol. Cell **13:**251–263.
46. **Nakashima, K., T. Hagiwara, A. Ishigami, S. Nagata, H. Asaga, M. Kuramoto, T. Senshu, and M. Yamada.** 1999. Molecular characterization of peptidylarginine deiminase in HL-60 cells induced by retinoic acid and 1α,25-dihydroxyvitamin D(3). J. Biol. Chem. **274:**27786–27792.
47. **Nakashima, K., T. Hagiwara, and M. Yamada.** 2002. Nuclear localization of peptidylarginine deiminase V and histone deimination in granulocytes. J. Biol. Chem. **277:**49562–49568.
48. **O'Brien, T., and J. T. Lis.** 1991. RNA polymerase II pauses at the 5′ end of the transcriptionally induced *Drosophila hsp70* gene. Mol. Cell. Biol. **11:**5285–5290.
49. **Pear, W. S., J. P. Miller, L. Xu, J. C. Pui, B. Soffer, R. C. Quackenbush, A. M. Pendergast, R. Bronson, J. C. Aster, M. L. Scott, and D. Baltimore.** 1998. Efficient and rapid induction of a chronic myelogenous leukemia-like myeloproliferative disease in mice receiving P210 bcr/abl-transduced bone marrow. Blood **92:**3780–3792.
50. **Phatnani, H. P., and A. L. Greenleaf.** 2006. Phosphorylation and functions of the RNA polymerase II CTD. Genes Dev. **20:**2922–2936.
51. **Pluquet, O., and P. Hainaut.** 2001. Genotoxic and non-genotoxic pathways of p53 induction. Cancer Lett. **174:**1–15.
52. **Richmond, T. J., and C. A. Davey.** 2003. The structure of DNA in the nucleosome core. Nature **423:**145–150.
53. **Sandal, T., L. Aumo, L. Hedin, B. T. Gjertsen, and S. O. Doskeland.** 2003. Irod/Ian5: an inhibitor of gamma-radiation- and okadaic acid-induced apoptosis. Mol. Biol. Cell **14:**3292–3304.
54. **Senese, S., K. Zaragoza, S. Minardi, I. Muradore, S. Ronzoni, A. Passafaro, L. Bernard, G. F. Draetta, M. Alcalay, C. Seiser, and S. Chiocca.** 2007. Role for histone deacetylase 1 in human tumor cell proliferation. Mol. Cell. Biol. **27:**4784–4795.
55. **Shilatifard, A.** 2006. Chromatin modifications by methylation and ubiquitination: implications in the regulation of gene expression. Annu. Rev. Biochem. **75:**243–269.
56. **Sims, R. J., III, R. Belotserkovskaya, and D. Reinberg.** 2004. Elongation by RNA polymerase II: the short and long of it. Genes Dev. **18:**2437–2468.
57. **Strahl, B. D., S. D. Briggs, C. J. Brame, J. A. Caldwell, S. S. Koh, H. Ma, R. G. Cook, J. Shabanowitz, D. F. Hunt, M. R. Stallcup, and C. D. Allis.** 2001. Methylation of histone H4 at arginine 3 occurs in vivo and is mediated by the nuclear receptor coactivator PRMT1. Curr. Biol. **11:**996–1000.
58. **Tang, Y., J. Luo, W. Zhang, and W. Gu.** 2006. Tip60-dependent acetylation of p53 modulates the decision between cell-cycle arrest and apoptosis. Mol. Cell **24:**827–839.
59. **Vogelstein, B., D. Lane, and A. J. Levine.** 2000. Surfing the p53 network. Nature **408:**307–310.
60. **Wang, H., W. An, R. Cao, L. Xia, H. Erdjument-Bromage, B. Chatton, P. Tempst, R. G. Roeder, and Y. Zhang.** 2003. mAM facilitates conversion by ESET of dimethyl to trimethyl lysine 9 of histone H3 to cause transcriptional repression. Mol. Cell **12:**475–487.
61. **Wang, H., Z. Q. Huang, L. Xia, Q. Feng, H. Erdjument-Bromage, B. D. Strahl, S. D. Briggs, C. D. Allis, J. Wong, P. Tempst, and Y. Zhang.** 2001. Methylation of histone H4 at arginine 3 facilitating transcriptional activation by nuclear hormone receptor. Science **293:**853–857.
62. **Wang, Y., J. Wysocka, J. Sayegh, Y. H. Lee, J. R. Perlin, L. Leonelli, L. S. Sonbuchner, C. H. McDonald, R. G. Cook, Y. Dou, R. G. Roeder, S. Clarke, M. R. Stallcup, C. D. Allis, and S. A. Coonrod.** 2004. Human PAD4 regulates histone arginine methylation levels via demethylimination. Science **306:**279–283.
63. **Waterman, M. J., E. S. Stavridi, J. L. Waterman, and T. D. Halazonetis.** 1998. ATM-dependent activation of p53 involves dephosphorylation and association with 14-3-3 proteins. Nat. Genet. **19:**175–178.
64. **Wei, C. L., Q. Wu, V. B. Vega, K. P. Chiu, P. Ng, T. Zhang, A. Shahab, H. C. Yong, Y. Fu, Z. Weng, J. Liu, X. D. Zhao, J. L. Chew, Y. L. Lee, V. A. Kuznetsov, W. K. Sung, L. D. Miller, B. Lim, E. T. Liu, Q. Yu, H. H. Ng, and Y. Ruan.** 2006. A global map of p53 transcription-factor binding sites in the human genome. Cell **124:**207–219.
65. **Xiong, Y., G. J. Hannon, H. Zhang, D. Casso, R. Kobayashi, and D. Beach.** 1993. p21 is a universal inhibitor of cyclin kinases. Nature **366:**701–704.